Human 3D Gastrointestinal Microtissue Barrier Function As a Predictor of Drug-Induced Diarrhea

Matthew F. Peters,[*,1] Tim Landry,[†] Carmen Pin,[‡] Kim Maratea,[*] Cortni Dick,[*] Matthew P. Wagoner,[*,2] Allison L. Choy,[§] Herb Barthlow,[*] Deb Snow,[*] Zachary Stevens,[†] Alex Armento,[†] Clay W. Scott,[*] and Seyoum Ayehunie[†]

[*]Oncology Safety, Drug Safety and Metabolism, IMED Biotech Unit, AstraZeneca, Waltham, MA 02451; [†]MatTek Corporation, Ashland, Massachusetts 01721; [‡]Mechanistic Safety and ADME Sciences, Drug Safety and Metabolism, IMED Biotech Unit, AstraZeneca, Cambridge, CB4 0WG, UK; and [§]Science and Enabling Units IT, AstraZeneca, Waltham, MA 02451

[1]To whom correspondence should be addressed at Oncology Safety, Drug Safety and Metabolism, IMED Biotech Unit, AstraZeneca, Boston, MA 02451. E-mail: matt.peters@astrazeneca.com.

[2]Present address: Takeda Pharmaceuticals, 35 Landsdowne St, Cambridge, MA 02139.

ABSTRACT

Drug-induced gastrointestinal toxicities (GITs) rank among the most common clinical side effects. Preclinical efforts to reduce incidence are limited by inadequate predictivity of *in vitro* assays. Recent breakthroughs in *in vitro* culture methods support intestinal stem cell maintenance and continual differentiation into the epithelial cell types resident in the intestine. These diverse cells self-assemble into microtissues with *in vivo*-like architecture. Here, we evaluate human GI microtissues grown in transwell plates that allow apical and/or basolateral drug treatment and 96-well throughput. Evaluation of assay utility focused on predictivity for diarrhea because this adverse effect correlates with intestinal barrier dysfunction which can be measured in GI microtissues using transepithelial electrical resistance (TEER). A validation set of widely prescribed drugs was assembled and tested for effects on TEER. When the resulting TEER inhibition potencies were adjusted for clinical exposure, a threshold was identified that distinguished drugs that induced clinical diarrhea from those that lack this liability. Microtissue TEER assay predictivity was further challenged with a smaller set of drugs whose clinical development was limited by diarrhea that was unexpected based on 1-month animal studies. Microtissue TEER accurately predicted diarrhea for each of these drugs. The label-free nature of TEER enabled repeated quantitation with sufficient precision to develop a mathematical model describing the temporal dynamics of barrier damage and recovery. This human 3D GI microtissue is the first *in vitro* assay with validated predictivity for diarrhea-inducing drugs. It should provide a platform for lead optimization and offers potential for dose schedule exploration.

Key words: gastrointestinal; toxicity; diarrhea; intestine; microtissue; enteroid; organoid.

Gastrointestinal toxicities (GITs) are among the most common drug adverse events (AE) in Phase 1 clinical trials (Federer *et al.*, 2016; Monticello *et al.*, 2017). Nausea, vomiting, constipation, and diarrhea all rank among the top seven drug-AEs (Federer *et al.*, 2016). These functional toxicities are in most instances nonlife-threatening. Consequently, the medical responses in clinical trials tend to focus on anti-diarrheal co-therapy and/or dose reduction (Al-Saffar *et al.*, 2015; Cook *et al.*, 2014). Such clinical management avoids drug attrition but carries significant burden for patient quality of life, compliance, and overall efficacy (Al-Saffar *et al.*, 2015). Ideally, GIT risks would be discovered and addressed preclinically. However, the

gastrointestinal tract is presently among the target organs least likely to result in attrition in either the preclinical or clinical phases (Cook *et al.*, 2014; Guengerich, 2011; Olson *et al.*, 2000; Stevens and Baker, 2009). New preclinical approaches are needed to allow earlier testing and selection of drugs with improved GI safety.

Current preclinical GI safety assessment depends on *in vivo* tests in higher-order species to achieve translational accuracy. Retrospective evaluation of compounds with clinical GI toxicity (100% prevalence), revealed that GIT in rodents had only 46% clinical concordance compared with 83% in nonrodents (Olson *et al.*, 2000). Conversely, when compounds with preclinical GIT were followed prospectively through the completion of Phase 1 trials, the diagnostic value of different species revealed a proportionate reduction in uncertainty of 15% and 28% in rat and dog respectively compared with 87% in primate studies (Monticello *et al.*, 2017). Due to both ethical and cost considerations, drug testing in higher-order species is often limited to the final candidate drug (CD). Whereas such testing in preclinical species can be informative for predicting clinical outcomes, it inherently lacks the capacity to select/design drug molecules with improved safety. Higher-order species testing and throughput for earlier screening are the principle bottlenecks limiting preclinical GIT cascades.

The breakthrough discovery of conditions for long-term culturing of intestinal stem cells as organoids has the potential to be transformative (Ootani *et al.*, 2009; Sato *et al.*, 2009). Previous *in vitro* GI models relied on single cell type monocultures. In contrast, organoid intestinal stem cells maintain a flow of cells continually differentiating into the diverse epithelial cell types which self-organize into villus- and crypt-like domains (Yin *et al.*, 2016). A defining feature of enteroids is their cyst-like structure with the apical side of the epithelia oriented inward. The first GI toxicity-relevant assay with enteroids capitalized on this structure. Increases in lumenly-directed chloride flux through the CFTR channel resulted in osmotic swelling quantifiable microscopically. Swelling offers a functional assay specifically for drug-induced secretory diarrhea (Dekkers *et al.*, 2013; Fujii *et al.*, 2016). Screening organoids for cytotoxicity and/or reduced cell growth by measuring ATP or MTT has shown promise with small sets of 3–4 oncology drugs (Grabinger *et al.*, 2014; Hoyle *et al.*, 2016). However, more extensive application for drug screening may require adaptations to address shortcomings stemming from the spherical nature of organoids which can limit drug penetration, drug washout, and selective drug application to either the apical or basal surfaces (Blutt *et al.*, 2017; Fatehullah *et al.*, 2016).

Techniques for preparing GI microtissues that are nonspherical have emerged by combining elements of the two seminal methodologies for long-term organoid culturing. Briefly, Kuo and colleagues (Li *et al.*, 2014, 2016; Ootani *et al.*, 2009) maintained organoids with a supporting layer of mesenchymal cells, culturing with an air-liquid interface (ALI) in collagen. Clevers and colleagues (Sato *et al.*, 2009) discovered a defined set of growth factors (EGF, R-spondin 1, and Noggin) that supported organoids in Matrigel. Recently, multiple laboratories have generated nonspherical GI microtissues by using these methods with transwell culturing (Boccellato *et al.*, 2018; Wang *et al.*, 2015, 2017) which is known to be an additional driver of morphological differentiation (Nossol *et al.*, 2011). These transwell cultures have the benefit of allowing for straightforward access to both basal and apical spaces. Here, we assessed a GI microtissue supported by fibroblast, cultured under ALI conditions in a transwell format. The selected model also meets essential screening needs of (1) human-derived cultures and (2) moderate throughput (96-well format).

Several key principles guided the selection of assay endpoints. First, Valentin and colleagues observed that most GI AEs are functional toxicities thereby suggesting that functional screening assays should be prioritized (Al-Saffar *et al.*, 2015). Second, assessing organ-specific cultures (hepatic-, cardiac-, and kidney-derived) using cytotoxicity endpoints have failed to accurately predict specific-organ clinical toxicities (Lin and Will, 2012), suggesting that GI-specific functional readouts should be employed. Third, clinical strategies for managing GIT exploit dose scheduling, thereby suggesting that kinetic data should be generated, if possible, to inform mathematical modeling and guide discovery of optimized clinical schedules (Gamucci *et al.*, 2014; Stein *et al.*, 2010). Consistent with each of these demands, TEER was selected as a nondestructive label-free measure of a core epithelial function and diarrhea was selected as a clinical AE that correlates with barrier dysfunction (Odenwald and Turner, 2017).

Here, we evaluated the predictive potential of changes in microtissue barrier function to screen drugs associated with clinical diarrhea. We further explored the response dynamics for features needed to support mathematical modeling used to guide mitigation strategies for drug-induced GIT.

MATERIALS AND METHODS

Tissue and fibroblast sources. The primary intestinal fibroblasts were purchased from Lonza (Cat No. CC-2902, Walkersville, Maryland). Primary human small intestine cells were obtained as previously described in Maschmeyer *et al.* (2015). Cells from the ileum region were obtained from a 19-year-old female donor with consent as previously described in Ayehunie *et al.* (2018). Cells were expanded and cryopreserved for future use.

Microtissue preparation. To reconstruct the 3D small intestinal microtissues, cryopreserved fibroblasts were thawed, expanded in DMEM supplemented with 10% fetal bovine serum, trypsinized, counted, and seeded (4.1×10^4 cells/cm^2) onto collagen coated 96-well plates (Millipore Corporation, 0.12 cm^2/well). The fibroblasts were incubated at 37°C for 4–6 h and primary human small intestinal epithelial cells were seeded and cultured in a SMI-100-FT-MM media (MatTek Corporation, Ashland, Massachusetts) for 4 days submerged, and for an additional 10 days at the ALI at 37°C, 5% CO$_2$ and 98% relative humidity. These transwell microtissues (termed SMI-100-FT or EpiIntestinal-FT) were fed basolaterally only during the ALI culture period. To keep the apical layer hydrated, 40 µl of medium (SMI-100-MM, MatTek Corporation) was added topically every other day. To complete cellular differentiation, cells were cultured for a total of 14 days prior to drug exposure.

Caco-2 culturing. Caco-2 cells were purchased (American Type Culture Collection [ATCC], Manassas, Virginia) and cultured according to the ATCC Product Sheet in Eagle's Minimum Essential Medium supplemented with 20% fetal bovine serum and incubated at 37°C. Cells were passaged until sufficient numbers allowed for experimental purposes, trypsinized, counted, and seeded (5×10^4 cells/well) onto collagen coated 96-transwell plates (Millipore Corporation, 0.12 cm^2/well). Within the transwell plates, cells were maintained using 250 and 100 µl complete media in the basolateral and apical chambers, respectively. TEER was monitored until a stable reading of $> 2\,500\ \Omega$ (approximately 14 days) was achieved.

Drug preparation and treatment. Validation drugs were purchased from MilliporeSigma (St. Louis, Missouri). AZD drugs were synthesized at AstraZeneca and were > 97% pure with no single impurity > 1%. Drugs stock solutions were prepared at 100 mM in DMSO. Dilutions were made in media yielding 0.1% DMSO final concentration. Drugs were washed out with three exchanges of media. No instances of washout-induced tissue damage were noted for either negative-control drugs or buffer-treated wells.

Histology and immunohistochemistry (IHC), and in-situ *hybridization (ISH).* Microtissues were fixed at room temperature in 10% neutral buffered formalin for approximately 24 h, routinely processed, embedded in paraffin blocks, sectioned at 4 μm, and stained with hematoxylin and eosin (H&E). All steps of the IHC and ISH procedures were performed on a Discovery Ultra automated slide staining system (Ventana Medical Systems, Tucson, Arizona). For both methods, serial tissue sections were placed on charged slides and dewaxed, followed by dehydration through a graded ethanol series.

For immunohistochemistry, tissue sections were subjected to heat-induced antigen retrieval, then incubated for 60 min with rabbit primary antibodies directed against Ki-67 (clone SP6, 1:250 dilution, Thermo Fisher Scientific, Waltham, Massachusetts), vimentin (clone D21H3, 1:100 dilution, Abcam, Cambridge, Massachusetts), villin-1 (clone SP145, 1:100 dilution, Abcam), and OLFM4 (clone D1E4M, 1:200 dilution, Cell Signaling Technology, Danvers, Massachusetts), or mouse primary antibodies directed against cytokeratins (clone AE1/AE3, 1:100 dilution, Thermo Fisher Scientific) and alpha smooth muscle actin (clone 1A4, 1:1000 dilution, Agilent Dako, Santa Clara, California). Immunoreactivity was detected with Discovery OmniMap anti-Rb or anti-Ms HRP (Ventana Medical Systems) and visualized with Discovery ChromoMap DAB (Ventana Medical Systems). Slides were counterstained with hematoxylin. Normal human small intestine was used as the positive control tissue.

The RNAScope ISH method was performed using the RNAScope VS Universal HRP Reagent Kit—Brown and probes against human Lgr5 (No. 311029), human PPIB (No. 313909, positive control probe), and bacterial dapB (No. 312039, negative control probe) (Advanced Cell Diagnostics, Hayward, California). Briefly, tissue sections were subjected to target retrieval (16 min at 97°C for microtissues and 40 min at 97°C for human small intestine), and protease treatment (16 min at 37°C). Hybridization with target probes, mRNA amplification and DAB chromogenic detection followed standard protocols established by Advanced Cell Diagnostics and Ventana Medical Systems. Slides were counterstained with hematoxylin. Normal human small intestine was used as the positive control tissue.

For image analysis, slides were scanned at ×20 magnification with an Aperio Versa scanner (Leica Biosystems, Buffalo Grove, Illinois). The percentage cellularity (positive cells/all nucleated cells) for Lrg5 and OLFM4 was calculated in the epithelial layer using HALO digital image analysis platform (Indica Labs, Corrales, New Mexico).

Transmission electron microscopy (TEM) and scanning electron microscopy (SEM). Ultrastructural features of the small intestinal tissues were examined by transmission electron microscopy (TEM) and scanning electron microscopy (SEM) using procedures as previously described in Ito and Karnovsky (1968). Briefly, tissues were fixed at room temperature for 2 h using 5% glutaraldehyde in 0.1 M sodium cacodylate buffer, pH 7.2 and post-fixed with 1% osmium tetroxide (OsO_4)/1.5% potassium ferrocyanide ($KFeCN_6$) for 1 h. Samples were washed in water (2×) and in 50 mM Maleate buffer pH 5.15 (MB) (1×), incubated in 1% uranyl acetate in MB for 1 h, and again washed in MB and water. Samples were dehydrated in a graded series of ethanol, placed in propyleneoxide for 1 h, and infiltrated with a 1:1 mixture of propyleneoxide and TAAB Epon (Marivac Canada, Inc, St. Laurent, Canada). Ultrathin sections (80 nm) were cut, picked up on to copper grids stained with lead citrate and examined using a JEOL 1200EX Transmission electron microscope at Harvard Medical School (Boston, Massachusetts). For SEM, following dehydration the samples were critically point dried and mounted onto specimen mounts using double sided carbon conductive adhesive. Samples were sputter coated with 5 nm platinum using a Cressington 208 HR sputter coater. Samples were viewed on a Hitachi S-4800 FESEM at Northeastern University (Boston, Massachusetts). Techniques described above were used to visualize ultrastructural features including the villi, brush borders, and tight junctions in the small intestinal microtissues.

Barrier integrity. Changes in barrier function of the microtissues were quantified using transepithelial electrical resistance (TEER) measurements. TEER monitors the presence of functional intercellular tight junctions which are responsible for the barrier function. TEER measurements were made using the EVOM volt-ohmmeter equipped with an STX-100 electrode (World Precision Instruments, Sarasota, Florida). Raw resistance measurements (Ω) were converted to TEER readings (Ω^*cm^2) by multiplying the raw readings for each tissue by the surface area of the cell culture inserts (0.12 cm^2) for the 96-well membrane bottom plate. TEER measurements were normalized as a percentage of the untreated control tissues: % TEER = TEER (Ω^*cm^2) of treated tissues (TTT) divided by the TEER of untreated tissues (TUT) times 100% TEER = (TTT/TUT)*100.

For TEER measurement, tissues were kept in TEER buffer for 30 min (an estimated processing time for TEER measurement of 96-well plate) at room temperature. Comparison of TEER values at 0 and 30 min time points in TEER buffer showed no significant difference. No edge effects were noted. Drugs were applied in 0.1% DMSO at the indicated final concentration on both apical and basolateral sides. DMSO alone had no effect on TEER. To avoid potential nonspecific osmotic effects associated with high concentrations of drug, 100 μM was set as the maximum concentration tested. Potency values were estimated using GraphPad PRISM 7.04 (La Jolla, California).

MTT viability assay. Tissue viability was determined using the MTT assay (3-(4,5-dimethylthiazole-2-yl)-2,5-diphenyl tetrazolium bromide; Cat No. M2128, Sigma-Aldrich, St. Louis, Missouri). After exposure to test drugs, the tissues were rinsed with PBS and then the tissues were placed in 100 μl of MTT dye loaded with MTT dye (1 mg/ml). The plates were then placed into a 37°C, 5% CO_2 incubator for 3 h. To stop the reaction and extract the formazan, the tissues were then transferred to a second 96-well plate containing 250 μl isopropyl alcohol (extractant). Additional 150 μl of extractant was added apically to the surface of the tissues. The 96-well plate was sealed in a plastic bag and the extraction was allowed to proceed overnight at room temperature in the dark. Afterwards, 200 μl of the formazan extract was quantified colometrically by measuring optical density (OD) at 570 nm in an E-MAX 96-well plate reader (Molecular Devices, Menlo Park, California). The tissue viability was determined by normalizing the OD for treated tissues as a percent of unexposed control tissues, which are loaded with MTT and extracted in an identical manner. Tissue viability (%)

was determined using the equation: % viability (OD of treated tissue)/(OD of control tissue)*100.

Mathematical modeling. The methods for modeling with AZD1, which showed diarrhea as the clinical DLT, included the base assumption consistent with our observations that the barrier damage associated with AZD1 exposure accumulates and reaches a threshold before TEER is affected. To explore this hypothesis, a nonautonomous system of differential equations was used to describe the temporal dynamics of the delayed TEER response to AZD1 exposure as follows:

$$\frac{dD}{dt} = k_{Di}\left(\frac{1}{1 + \frac{C_S}{C}}\right),$$ (1)

$$\frac{dT}{dt} = -k_{Td}\left(\frac{1}{1 + \left(\frac{D_{Thr}}{D}\right)^n}\right)\left(1 - \frac{T_{Min}}{T}\right).$$ (2)

The variable $D(t)$ in equation 1 quantifies the accumulated barrier damage at time t in response to AZD1 exposure; the parameter C_S of the scaling function, determines the potency at which AZD1 concentration, $C(t)$, is mapped into the interval $(0, 1)$ by the hill function; $k_{Di} > 0$ is the rate of damage accumulation during AZD1 exposure. The variable $T(t)$ in equation 2 denotes TEER (%); $T_{Min} \leq T(0)$ is the minimum TEER value whereas $k_{Td} > 0$ is the rate of TEER loss associated with barrier damage. The parameter D_{Thr} denotes the barrier damage threshold for TEER to be affected and n regulates the steepness of the system transition when D reaches D_{Thr}.

Supplementary Table 1 shows the values identified for the model parameters. T_{min} was given a fixed value equal to 20, which was derived from our experimental observations, whereas a fixed value of n equal to 10 was suitable for model fitting purposes and enabled rapid TEER transition between states once the threshold was reached. The unambiguous identification of the values of the parameters k_{Di} and D_{Thr} in equations 1 and 2, requires information on the dynamics of the barrier damage, which is missing in our experimental setting. To circumvent this lack of knowledge, it was arbitrarily assumed that the rate of damage accumulation was equal to 1, $k_{Di} = 1$. The value for k_{Di} affects the value of D_{Thr} and the scale of $D(t)$, which quantifies a barrier damage of unknown nature, but it does not affect the values of the rest of model parameters. Under these assumptions and with $T(0)=100$ and $D(0)=0$ as initial values for T and D, respectively, the values of D_{Thr}, k_{Td}, and C_S were identified by fitting equations 1 and 2 to our datasets generated with 4 doses and 3 time schedules as described above.

The nonautonomous system described in equations 1 and 2 was extended to incorporate TEER recovery dynamics. TEER was assumed to recover after the barrier damage, D, is repaired and reaches values below the threshold D_{Thr} as follows:

$$\frac{dD}{dt} = -k_{Dd}D + k_{Di}\left(\frac{1}{1 + \frac{C_S}{C}}\right),$$ (3)

$$\frac{dT}{dt} = -k_{Td}\left(\frac{1}{1 + \left(\frac{D_{Thr}}{D}\right)^n}\right)\left(1 - \frac{T_{min}}{T}\right) + k_{Ti}T\left(1 - \frac{T}{T_{max}}\right)\left(1 - \frac{T_{min}}{T}\right)\left(1 - \frac{1}{1 + \left(\frac{D_{Thr}}{D}\right)^n}\right),$$ (4)

where k_{Dd} is the repair rate of the barrier damage; k_{Ti} is the rate at which TEER recovers once the damage is below the threshold; $T_{max} > T_{min}$ is the maximum value TEER can reach.

The values of the repair associated model parameters, k_{Ti} and k_{Dd}, were estimated by fitting equations 3 and 4 to the dataset exhibiting TEER recovery obtained under the highest dose of AZD1, 100 μM, and with the longest off-period schedule, 5 days-on/9 days-off (Supplementary Table 1). A fixed value of T_{max} equal to 100 was assumed and used the values of the parameters previously estimated with equations 1 and 2 were used.

Whereas the TEER recovery rate, k_{Ti}, was unambiguously estimated with that dataset, the identified value for the damage repair rate, k_{Dd}, was strongly dependent on the value of the damage accumulation rate, k_{Di}, which was arbitrarily chosen as explained above. Thus, the true values for these parameters are to be identified in future work involving the understanding of the damage underlying TEER response. Parameter estimation, performed using nonlinear least squares methods (Marquardt algorithm), and model simulation were carried out using SAS 9.4.

RESULTS

Human GI microtissues were constructed by seeding small intestinal epithelial cells on a supportive layer of fibroblasts. Development and differentiation was induced by transwell culturing under ALI conditions (Figure 1A). Mature microtissues were composed of a monolayer of simple columnar epithelial cells with basally positioned nuclei, consistent with enterocytes. Microtissues formed occasional raised or fold-like structures and were supported by a connective tissue layer populated by fibroblasts (Figure 1B). Higher resolution images revealed that individual epithelial cells developed microvilli-like projections (Figure 1C). Presence of a continuous brush border was further supported by immunolabeling of villin on the epithelial surface (Figure 2A). Expression of claudin-1 confirmed tight junction formation between adjacent enterocyte cells (Figure 2B), which also stained positive for cytokeratins (Supplementary Figure 1). An average of 1.24 ± 0.68% ($n = 4$) of Lgr5-positive stem cells were distributed in pairs or single cells, at irregular intervals along the epithelium, paired or in small clusters (Figure 2C). A similar staining frequency and pattern (2.4 ± 2.4%, $n = 4$) was observed with a second stem cell marker, OLFM4 (Supplementary Figure 1). Because proliferating cells identified by Ki-67 immunolabeling (Figure 2D) were more numerous than stem cells, the majority were presumed to function as transit amplifying cells. The presence of fibroblasts and myofibroblasts in the connective tissue layer was confirmed by immunolabeling of vimentin (Figure 2E) and smooth muscle actin (Figure 2F), respectively.

Transwell microtissue barrier function was assessed by TEER. EpiIntestinal TEER values (150Ω/cm²) were lower than Caco-2 cultures (450Ω/cm²) under similar conditions. This may reflect uniform tight junctions in a Caco-2 monoculture compared with microtissues which include diverse intestinal types some of which lack tight junctions. These lower TEER values more closely align with measurements using native tissue (reviewed in [Srinivasan *et al.*, 2015]).

To test GI microtissue barrier function as a predictive correlate for clinical diarrhea, we assembled a set of validation compounds utilizing the following selection cascade. Lists of widely prescribed drugs were evaluated to ensure that clinical diarrhea incidence was based on sufficiently large sample sizes. For non-diarrheagenic drugs, upper limit for diarrhea incidence was set at 3% based on the rate of diarrhea in the general population, estimated at 3.2%–8.5% depending on symptom intensity (Rief *et al.*, 2006). For diarrheagenic drugs, lower limit for diarrhea
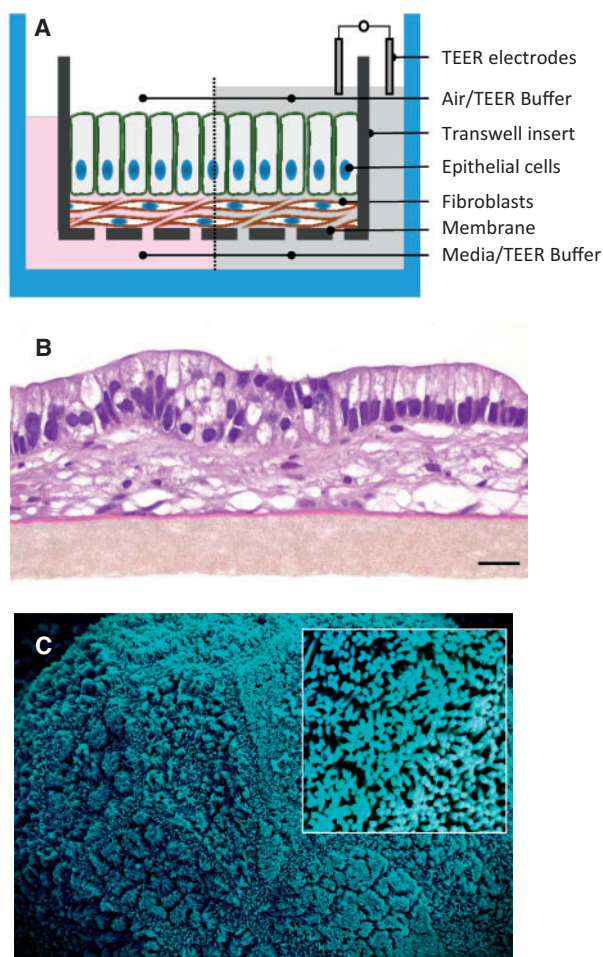
Figure 1. Format of human ileal microtissue. A, Schematic representation of EpiIntestinal microtissue for TEER analysis. Cultures were matured under ALI conditions (left). For TEER measurement, buffer was added to the apical surface and exchanged for media in the basal compartment (right). B, Representative section of microtissue stained with H&E (Scale bar = 50 μm). C, Scanning electron micrograph showing the surface structure of an EpiIntestinal villus (×5000 mag.) and microvilli (inset, ×25 000 mag.).

incidence was set at 40% to exclude the high background in some cancer patient placebo groups with incidence of 29.8% (95% CI of 22.9%–37.7%) (Llavero-Valero et al., 2016). Next, antibacterial agents were excluded because induction of diarrhea is secondary to disruption of commensal bacteria and subsequent *Clostridium difficile* colitis (Abraham and Sellin, 2012). Finally, agents inducing diarrhea by osmotic mechanisms such Mg^{++} salts and glycols were also excluded because these are well understand and predictable (Abraham and Sellin, 2007). This yielded a validation set of 39 drugs clearly discernable with respect to diarrhea responses in humans (Tables 1 and 2, and Supplementary Table 2).

Clinical exposure data was extracted from published literature. Total plasma C_{max} values were collected for the dose associated with incidence of diarrhea although this was not always available from studies associated with adverse events/diarrhea. Data were reviewed and best estimates for exposure values were determined prior to *in vitro* testing (Tables 1 and 2).

Drugs were tested at four concentrations (1, 5, 25, 100 μM) in the GI microtissue barrier function assay under blinded conditions (Figure 3A). TEER values were obtained after 48 h and 96 h of continuous drug exposure. Whereas TEER is a widely

accepted quantitative technique to measure the integrity of tight junction dynamics in cell culture models (Srinivasan et al., 2015), it also captures cytotoxic barrier disruption (Konsoula and Barile, 2007). Therefore, IC_{15} and IC_{25} were calculated, representing the lowest drug concentration that elicits measurable reduction. This also enabled quantifying activity with compounds where < 50% inhibition was observed at the highest test concentration.

To evaluate clinical translation, TEER potencies were normalized to the clinical exposure associated with diarrhea (total plasma C_{max}). The resulting TEER potency/clinical exposure ratios were examined seeking a threshold that might segregate diarrheagenic and nondiarrheagenic drugs. Predictive performance assessment by ROC analysis at three time-potencies (96h-IC_{15}, 96h-IC_{25}, and 48h-IC_{15}) revealed areas under the curve of 0.79, 0.76, and 0.67, respectively (Figure 3B). 96h-IC_{15} was chosen as the minimum disruption in barrier function. Under these conditions, nondiarrheagenic drugs were less potent and most (15 of 17) had TEER IC_{15}/exposure ratios > 80 (Figure 3C). Conversely, diarrheagenic drugs were more potent in TEER and most (11 of 14) had TEER IC_{15}/exposure ratios < 80. Peak predictivity was calculated to be at an 83-fold TEER IC_{15}/C_{max} ratio although similar predictivity spanned a range from 60 to 100 (Figure 3D, Youden Index analysis [Youden, 1950]). The pretest selection of 100 μM as the top testing concentration combined with the experimentally selected scoring criteria of 80-fold clinical C_{max} resulted in 8 of 39 drugs being un-scorable. These were inactive but were not tested up to the 80-fold C_{max} (Supplementary Table 3).

The selected conditions were tested in a repeat experiment, also under blinded-conditions. The predictive accuracy of the initial and repeat experiments were 84% and 83%, respectively (Tables 3 and 4). Assessment using an MTT assay was included as a measure of changes in cell metabolic activity and loss of viable cells. MTT yielded a 70% accuracy but only 50% sensitivity (Table 4). The validation set was also tested on Caco-2 cells where TEER responses exhibited 77% accuracy but only 57% sensitivity (Table 4); performance insufficient to meet standards for drug screening (Genschow et al., 2002).

To further explore translation, test compounds were sought for which diarrhea significantly impacted clinic trials as either the dose-limiting toxicity (DLT) or the most prevalent AE. In the AstraZeneca collection, four compounds were identified (AZD3409, AZD8931, AZD7140, and AZD3) that met these criteria and for which clinical exposure and preclinical animal data were also available (Appels et al., 2008; Johnston et al., 2016). These compounds were tested for effects on TEER in the human microtissue under blinded conditions. The TEER IC_{15}/clinical C_{max} ratios were ≤ 8 for all four compounds (Table 5), ie, all four were active in the human microtissue assay.

For therapeutic areas such as oncology, where GIT is often mediated by an on-target mechanism, mitigation of the adverse event risk is not possible through compound screening during drug discovery. In such cases, a commonly utilized approach is to design dosing schedules that maximize therapeutic index, a process that can be informed by mathematical modeling (Cadoo et al., 2016; Shankaran et al., 2018). Such modeling often requires time-series data, a requirement that is well-aligned with the label-free and nondestructive nature of TEER. To investigate the ability of GI microtissue TEER to inform the dynamics of tissue damage in this system, a feasibility study was undertaken with multiple rounds of repeat treatment and washout over an extended period. The pilot test explored response kinetics using a proprietary candidate drug (AZD1) which was dose-limited by
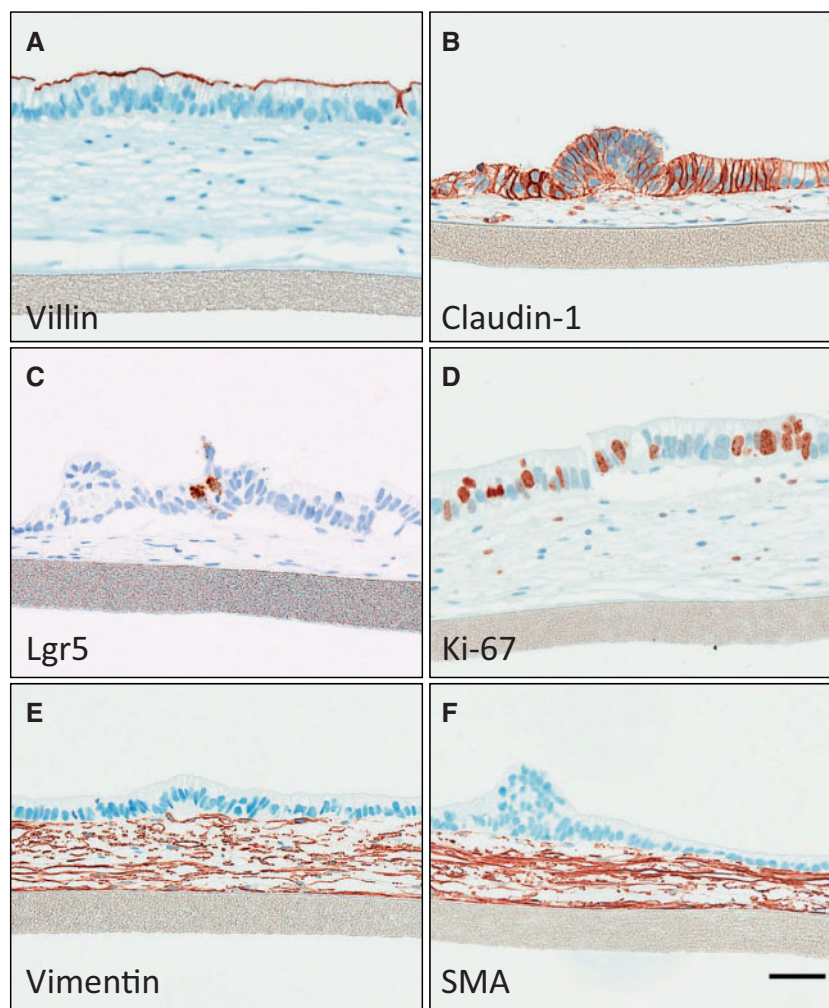
Figure 2. Immunohistochemical phenotyping of human ileal microtissues. A, Continuous villin immunostaining (brown) on the epithelial surface confirmed the presence of a brush border. B, Tight junctions identified by distinct membrane staining of Claudin-1 in enterocytes. C, Few Lgr5-positive stem cells interspersed among enterocytes. D, Proliferating cells identified by nuclear staining of Ki-67. E, Vimentin immunostaining in fibroblasts. F, Smooth muscle actin immunostaining demonstrates myofibroblast phenotype (Scale bar = 50 μm).

diarrhea. A second proprietary candidate drug (AZD2) which was not clinically limited by diarrhea was intended as a negative control whereas AZD8391 was included as a positive control. Compounds were tested at 100 μM concentration, which aligns with the predicted peak intestinal concentrations. Microtissues were incubated with test compounds for 3 days followed by a wash out, whereas TEER was measured daily (Figure 4). AZD1 and AZD8391, but not AZD2, caused a pronounced decrease in TEER during the 3-day treatment period. AZD8931-treated microtissue quickly recovered TEER after washout whereas microtissue treated with AZD1 recovered slowly over 17 days. A second treatment cycle resulted in either slower or no recovery for AZD8391 and AZD1, respectively. This apparent sensitization of the tissue for drug effects did not occur with other toxicants (not shown), suggesting a specific effect of these two compounds on microtissue barrier function. This contrasts with AZD2 where repeat exposures had no effect on TEER. The precision observed across repeat drug exposure and washout over 42 days suggests the data can resolve barrier function dynamics for mathematical modeling.

Whereas the data in Figure 4 demonstrated the capacity to resolve response kinetics, building models based on continuous in vitro exposure will likely give suboptimal clinical translation and may in some instances create irrelevant in vitro toxicity due to artificially high drug exposures. Therefore, to explore the ability of microtissue TEER data to inform a dynamic model of GIT, AZD1 was reevaluated with drug exposures tailored to replicate the clinical setting. SimCYP software was used to estimate the human intracellular enterocyte exposure of AZD1 after an oral 75 mg dose. This revealed a transient exposure with a midpoint concentration lasting for approximately 150 min (data not shown). Microtissues were treated with AZD1 for 150 min each day according to three clinical dosing schedules: 3 days-on/4 days-off, 5 days-on/2 days-off, and 5 days-on/9 days-off. Four concentrations (5, 20, 50, and 100 μM) covering the predicted enterocyte exposures were tested on each schedule (Figure 5). The raw TEER data suggested two trends: (1) the disruption of TEER was delayed in an exposure-related fashion and (2) the recovery of TEER takes longer than the longest off-period schedule, 5 days-on/9 days-off, at the highest dose (Figure 5).

To link the dynamic exposure and TEER response quantitatively, a mathematical model was developed using a nonautonomous system of differential equations (equations 1 and 2). Following raw data observations, the model was designed based

Table 1. Marketed Drugs With Limited Incidence of Clinical Diarrhea

Drug Name	Diarrhea Incidence	Reference	Clinical C_{max} (M)	Reference
Acetaminophen	1%	Acetaminophen. Sider 8.1: Side Effect Resource. http://sideeffects.embl.de/drugs/1983/. Retrieved September 10, 2018	1.4E-04	Acetaminophen. McNeil's background package on acetaminophen for the September 19, 2002 Nonprescription Drugs Advisory Committee Meeting. https://wayback.archive-it.org/7993/20170405154808/https://www.fda.gov/ohrms/dockets/ac/02/briefing/3882B1_13_McNeil-Acetaminophen.htm#_Toc18717571. Accessed September 6, 2018
Verapamil	2%	Verapamil. Sider 4.1: Side Effect Resource. http://sideeffects.embl.de/drugs/2520/. Retrieved September 10, 2018	9.9E-08	Br. J. Clin. Pharmacol. **33**, 623–627 (1992)
Dofetilide	3%	Dofetilide. Sider 4.1: Side Effect Resource. http://sideeffects.embl.de/drugs/71329/. Retrieved September 10, 2018	8.6E-09	Br. J. Clin. Pharmacol. **50**, 247–253 (2000)
Amiodarone	< 2%	Amiodarone. Sider 4.1: Side Effect Resource. http://sideeffects.embl.de/drugs/2156/. Retrieved September 10, 2018	4.7E-06	Circulation **67**, 1347–1355 (1983)
Fondaparinux	< 3%	Fondaparinux. Sider 8.1: Side Effect Resource. http://sideeffects.embl.de/drugs/123611/. Retrieved September 10, 2018	8.4E-07	Clin. Pharmacokinet. **41**(Suppl. 2), 1–9 (2002)
Alfuzosin	Not noted	http://sideeffects.embl.de/	3.2E-08	Alfuzosin Hydrochloride. Mosby's Drug Consult. (2006). https://www.pharmapendium.com/#/browse/mosby/Alfuzosin%20Hydrochloride/Alfuzosin%20Hydrochloride
Triamcinolone	Not noted	http://sideeffects.embl.de/	2.7E-08	Whelan, G. J., Szefler, S. J. (2006). Asthma management. In Applied Pharmacokinetics & Pharmacodynamics, 4th ed. (M. E. Burton, Ed.), pp. 259–263. Lipincott Williams & Wilkins
Ranolazine	Not noted	http://sideeffects.embl.de/	1.4E-05	Ranolazine. Mosby's Drug Consult. (2006). https://www.pharmapendium.com/#/browse/mosby/Ranolazine/Ranolazine
Fomepizole	Not noted	http://sideeffects.embl.de/	2.1E-04	Fomepizole. Mosby's Drug Consult. (2006). https://www.pharmapendium.com/#/browse/mosby/Fomepizole/Fomepizole
Haloperidol	Not noted	http://sideeffects.embl.de/	2.7E-08	Clin. Pharmacokinet. **34**, 227–263 (1998)
Isoprenaline	Not noted	http://sideeffects.embl.de/	2.7E-09	Br. J. Pharmacol. **46**, 458–472 (1972)
Amlodipine	Not noted	http://sideeffects.embl.de/	1.0E-08	Clin. Pharmacokinet. **22**, 22–31 (1992)
Dexamethasone	Not noted	http://sideeffects.embl.de/	1.6E-07	Br. J. Clin. Pharmacol. **78**, 78–83 (2013)
Finasteride	Not noted	http://sideeffects.embl.de/	2.2E-07	Clin. Pharmacokinet. **30**, 16–27 (1996)
Nadolol	Not noted	http://sideeffects.embl.de/	4.3E-07	Eur. J. Clin. Pharmacol. **26**, 125–127 (1984)
Nifedipine	Not noted	http://sideeffects.embl.de/	4.6E-07	Hypertension **5**, II18–II24 (1983)
Methoxsalen	Not noted	http://sideeffects.embl.de/	1.5E-06	Clin. Pharmacol. Ther. **25**, 167–171 (2016)
Flecainide	Not noted	http://sideeffects.embl.de/	9.3E-07	Clin. Pharmacol. Ther. 72, 112-22 (2002)
Maprotiline	Not noted	http://sideeffects.embl.de/	2.3E-07	Br. J. Clin. Pharmacol. **37**, 383–388 (1994)
Dexmedetomidine	Not noted	http://sideeffects.embl.de/	4.7E-09	Br. J. Anaesth. **88**, 669–675 (2002)
Furosemide	Not noted	http://sideeffects.embl.de/	6.7E-06	Clin. Pharmacol. Ther. **14**, 178–186 (1974)

Table 2. Marketed Drugs With Clinical Diarrhea Incidence

Drug Name	Diarrhea Incidence	Reference	Clinical C_{max} (M)	Reference
Afatinib	96%	Afatinib Dimaleate. FDA Approval Package (07/2013). NDA 201292/S001. https://www.pharmapendium.com/#/browse/fda/Afatinib%20Dimaleate/36c1e712fe5b80809bd835499e2c359f?reference=12	7.8E-08	*Clin. Pharmacokinet.* **52**, 1101 (2013)
Colchicine	77%	Colchicine. FDA Approval Package (07/2009). Label 022351/S000. https://www.pharmapendium.com/#/browse/fda/Colchicine/62d41b1153aa9960e19-c6a2a2a0b238b? reference=7	1.7E-08	Colchicine. FDA Approval Package (07/2009). Label 022351/S-000. https://www.pharmapendium.com/#/browse/fda/Colchicine/62d41b1153aa9960e19-c6a2a2a0b238b? reference=7
Idarubicin	73%	Idarubicin Hydrochloride. Mosby's Drug Consult. (2006). https://www.pharma-pendium.com/#/browse/mosby/Idarubicin%20Hydrochloride/Idarubicin%20Hydrochloride#t003013-ar-2	8.8E-08	*Br. J. Clin. Pharmacol.* **23**, 303–310 (1987)
Tacrolimus	72%	Tacrolimus. Mosby's Drug Consult. (2006). https://www.pharmapendium.com/#/browse/mosby/Tacrolimus/Tacrolimus#s003138-ar-lfrar	8.3E-08	Tacrolimus. Mosby's Drug Consult. (2006). https://www.pharmapen-dium.com/#/browse/mosby/Tacrolimus/Tacrolimus
Imatinib	60%	Imatinib Mesylate. Mosby's Drug Consult. (2006). https://www.pharmapendium.com/#/browse/mosby/Imatinib%20Mesylate/Imatinib%20Mesylate#s003519-ar	3.2E-06	*Clin. Pharmacokinet.* **44**, 879–894 (2005)
Capecitabine	55%	Capecitabine. Mosby's Drug Consult. (2006). https://www.pharmapendium.com/#/browse/mosby/Capecitabine/Capecitabine	9.7E-06	*Clin. Pharmacokinet.* **40**, 85–104 (2001)
Axitinib	54%	Axitinib. FDA Approval Package (2011-04-14). Medical/Clinical Review. NDA 202324/S-000 Part 05. https://www.pharmapendium.com/#/browse/fda/Axitinib/4732e3524b795cb6ae3100690e755c8b?reference=22	5.6E-08	*Clin. Pharmacokinet.* **52**, 713–725 (2013)
Bortezomib	51%	Bortezomib. Mosby's Drug Consult. (2006). https://www.pharmapendium.com/#/browse/mosby/Bortezomib/Bortezomib	1.3E-06	Bortezomib. Mosby's Drug Consult. (2006). https://www.pharmapen-dium.com/#/browse/mosby/Bortezomib/Bortezomib
Prostacyclin	50%	Epoprostenol Sodium. Mosby's Drug Consult. (2006) .https://www.pharma-pendium.com/#/browse/mosby/Epoprostenol%20Sodium/Epoprostenol%20Sodium	9.9E-10	*Br. J. Clin. Pharmacol.* **74**, 978–989 (2012)
Crizotinib	49%	Crizotinib. FDA Approval Package (2011-08-26). Label 202570/S-000. https://www.pharmapendium.com/#/browse/fda/Crizotinib/39b826d9049e790c-f352ec46730b5ca6? reference=5	2.2E-07	*Am. J. Health Syst. Pharm.* **70**, 943–947 (2013)
Sorafenib	43%	Sorafenib Tosylate. Mosby's Drug Consult. (2006). https://www.pharmapendium.com/#/browse/mosby/Sorafenib%20Tosylate/Sorafenib#s004100-desc	6.2E-06	*Ann. Oncol.* **16**, 1688–1694 (2005)
Docetaxel	42%	Docetaxel. Mosby's Drug Consult. (2006). https://www.pharmapendium.com/#/browse/mosby/Docetaxel/Docetaxel#t003205-ar-14	3.7E-06	*BMC Cancer* **7**, 197 (2007)
Diacerein	41%	Dougados, M., Pham, T., Le Henanff, A., Ravaud, Ph., Dieppe, P., and Paolozzi, L. *Ann. Rheum. Dis.* **63**, 1611–1617 (2004).	1.3E-05	*Clin. Pharmacokinet.* **35**, 347–359 (1998)

Table 2. (continued)

Drug Name	Diarrhea Incidence	Reference	Clinical C_{max} (M)	Reference
Quinidine	40%	The Flecainide-Quinidine Research Group. *Circulation* **67**, 1117–1123 (1983).	1.2E-05	Quinidine Sulfate. Mosby's Drug Consult. (2006). https://www.pharmapendium.com/#/browse/mosby/Quinidine%20Sulfate/Quinidine%20Sulfate
Miglustat	89%	Miglustat. Mosby's Drug Consult. (2006). https://www.pharmapendium.com/#/browse/mosby/Miglustat/Miglustat	6.1E-06	*J. Clin. Pharmacol.* **47**, 1277–1282 (2007)
Metformin	53%	Metformin Hydrochloride. Mosby's Drug Consult. (2006) .https://www.pharmapendium.com/#/browse/mosby/Metformin%20Hydrochloride/Metformin%20Hydrochloride	8.9E-06	Metformin Hydrochloride. Mosby's Drug Consult. (2006). https://www.pharmapendium.com/#/browse/mosby/Metformin%20Hydrochloride/Metformin%20Hydrochloride
Stavudine	50%	Stavudine. Mosby's Drug Consult. (2006). https://www.pharmapendium.com/#/browse/mosby/Stavudine/Stavudine	2.4E-06	Stavudine. Mosby's Drug Consult. (2006). https://www.pharmapendium.com/#/browse/mosby/Stavudine/Stavudine
Mycophenolate mofetil	48%	Mycophenolate Mofetil. Mosby's Drug Consult. (2006). https://www.pharmapendium.com/#/browse/mosby/Mycophenolate%20Mofetil/Mycophenolate%20Mofetil	5.7E-05	Mycophenolate Mofetil. Mosby's Drug Consult. (2006). https://www.pharmapendium.com/#/browse/mosby/Mycophenolate%20Mofetil/Mycophenolate%20Mofetil

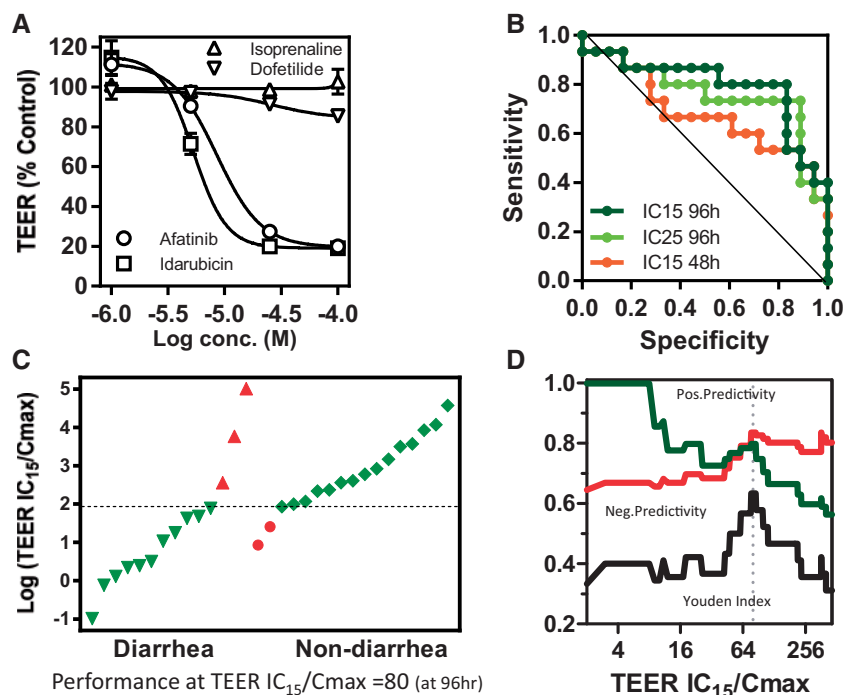

Figure 3. TEER responses of human GI microtissue to a panel of compounds with different diarrhea-genic risk. Four concentrations (1, 5, 25, 100 μM) were tested. A, Representative responses at 96 h are shown. Drugs reducing TEER by less than 15% were recorded as $IC_{15} > 100$ μM (Table 3, microtissue experiment 1). Error bars are standard deviation from two microtissues. B, Receiver-operating curves were plotted to examine the relative diagnostic value at 48 h versus 96h treatment and IC_{15} versus IC_{25}. Prediction outcomes were scored using a diarrhea-genic criteria of IC_{15}/C_{max} or $IC_{25}/C_{max} < 80$. C, TEER potencies (96h IC_{15}) were plotted as a ratio to clinical C_{max}. D, Predictivity metrics were plotted across TEER IC_{15}/C_{max} ratios.

on the assumptions that damage to the barrier cells accumulates with exposure to AZD1 and that TEER is affected only after the barrier damage reaches a threshold. Similar model architectures have been employed to quantify drug-induced damage and functional impairment in other tissues with laminar structure (Gebremichael *et al.*, 2018). A consistent threshold value linking damage and barrier function was able to explain the TEER measurements observed with diverse doses and

Table 3. Human GI Microtissue and Caco-2 Responses to Panel of Diarrhea Drugs

Drug Name	Clinical C_{max} (M)	Microtissue Exp 1			Microtissue Exp 2						Caco-2		
		TEER IC15	IC15/C_{max}	Predictive Outcome	TEER IC15	IC15/C_{max}	Predictive Outcome	MTT IC50	IC50/C_{max}	Predictive Outcome	TEER IC15	IC15/C_{max}	Predictive Outcome
Prostacyclin	9.9E-10	> 1.0E-04	101441	FN	> 1.0E-04	101441	FN	> 1.0E-04	101441	FN	> 1.0E-04	101441	FN
Colchicine	1.7E-08	> 1.0E-04	5874	FN	1.0E-06	59	TP	> 1.0E-04	5874	FN	1.0E+00	5874	FN
Tacrolimus	8.3E-08	3.0E-05	363	FN	4.0E-05	484	FN	5.5E-05	665	FN	3.0E-05	363	FN
Afatinib	7.8E-08	6.0E-06	77	TP	8.5E-06	109	FN	3.0E-05	385	FN	9.0E-06	115	FN
Axitinib	5.6E-08	1.0E-06	18	TP	> 1.0E-04	1773	FN	> 1.0E-04	1773	FN	0.0E+00	1773	FN
Idarubicin	8.8E-08	4.3E-06	48	TP	2.5E-06	28	TP	1.0E-05	114	FN	8.0E-06	91	FN
Crizotinib	2.2E-07	9.5E-06	43	TP	9.5E-06	43	TP	2.2E-05	99	TP	8.0E-06	36	TP
Docetaxel	3.7E-06	4.0E-05	11	TP	4.0E-05	11	TP	6.5E-05	17	TP	1.0E-04	27	TP
Diacerein	1.3E-05	4.0E-05	3	TP	4.0E-05	3	TP	6.5E-05	5	TP	> 1.0E-04	8	TP
Quinidine	1.2E-05	3.0E-05	2	TP	3.0E-05	2	TP	> 1.0E-04	8	TP	> 1.0E-04	8	TP
Imatinib	3.2E-06	7.0E-06	2	TP	8.0E-06	2	TP	6.5E-05	20	TP	2.0E-05	6	TP
Sorafenib	6.2E-06	7.9E-06	1	TP	7.9E-06	1	TP	6.5E-05	11	TP	1.5E-05	2	TP
Bortezomib	1.3E-06	1.0E-06	1	TP	1.0E-06	1	TP	> 1.0E-04	75	TP	1.0E-06	1	TP
Capecitabine	9.7E-06	1.0E-06	0.1	TP	1.0E-06	0.1	TP	> 1.0E-04	10	TP	> 1.0E-04	10	TP
Isoprenaline	2.7E-09	> 1.0E-04	37533	TN	> 1.0E-04	37533	TN	> 1.0E-04	37533	TN	> 1.0E-04	37533	TN
Dofetilide	8.6E-09	> 1.0E-04	11620	TN	> 1.0E-04	11620	TN	> 1.0E-04	11620	TN	> 1.0E-04	11620	TN
Dexmedetomidine	4.7E-09	4.0E-05	8455	TN	4.0E-05	8455	TN	> 1.0E-04	21138	TN	> 1.0E-04	21138	TN
Triamcinolone	2.7E-08	> 1.0E-04	3756	TN	> 1.0E-04	3756	TN	> 1.0E-04	3756	TN	> 1.0E-04	3756	TN
Alfuzosin	3.2E-08	> 1.0E-04	3132	TN	> 1.0E-04	3132	TN	> 1.0E-04	3132	TN	> 1.0E-04	3132	TN
Amlodipine	1.0E-08	1.5E-05	1479	TN	1.0E-05	986	TN	4.5E-05	4438	TN	3.0E-05	2959	TN
Haloperidol	2.7E-08	2.2E-05	834	TN	8.0E-06	301	TN	9.0E-05	3382	TN	3.0E-05	1127	TN
Dexamethasone	1.6E-07	> 1.0E-04	609	TN	> 1.0E-04	609	TN	> 1.0E-04	609	TN	> 1.0E-04	609	TN
Verapamil	9.9E-08	4.0E-05	404	TN	4.5E-05	455	TN	> 1.0E-04	1011	TN	4.0E-05	404	TN
Finasteride	2.2E-07	8.0E-05	366	TN	> 1.0E-04	457	TN	> 1.0E-04	457	TN	> 1.0E-04	457	TN
Nadolol	4.3E-07	> 1.0E-04	234	TN	> 1.0E-04	234	TN	> 1.0E-04	234	TN	> 1.0E-04	234	TN
Nifedipine	4.6E-07	> 1.0E-04	216	TN	> 1.0E-04	216	TN	> 1.0E-04	216	TN	> 1.0E-04	216	TN
Fondaparinux	8.4E-07	> 1.0E-04	118	TN	> 1.0E-04	118	TN	> 1.0E-04	118	TN	> 1.0E-04	118	TN
Methoxsalen	1.5E-06	1.5E-04	100	TN	1.5E-04	100	TN	1.5E-04	100	TN	1.5E-04	100	TN
Flecainide	9.3E-07	8.0E-05	86	TN	> 1.0E-04	107	TN	> 1.0E-04	107	TN	> 1.0E-04	107	TN
Maprotiline	2.3E-07	6.0E-06	26	FP	9.0E-06	39	FP	6.5E-05	279	TN	3.0E-05	129	TN
Amiodarone	4.7E-06	4.0E-05	9	FP	N/T	—	—	N/T	—	—	3.3E-05	7	FP

Predictive outcomes were scored with using TEER IC$_{15}$/C$_{max}$ ratio < 80 as diarrhea-genic criteria. Each experiment was conducted under blinded conditions.

FN, false negative; FP, false positive; TN, true negative; TP, true positive.

schedules (mean = 0.48 ± 0.011, arbitrary units, see Supplementary Table 1).

In addition, we explored whether the damage-threshold model could be extended to include recovery of damage and TEER impairment. Equations 3 and 4 describe the extended system modeling the assumption that TEER recovers after the barrier damage is repaired sufficiently to fall below the threshold value. The values of the parameters governing the dynamics of damage accumulation and repair were identified using the 5 days-on/9 days-off schedule exhibiting recovery and enabled model predictions of TEER over time at all dose schedules (Figure 5). Future work exploring longer dose holidays will be needed to accurately inform the dynamics of tissue recovery.

DISCUSSION

GI AEs are the most common clinical side effects, yet there are no *in vitro* GIT assays validated for routine preclinical screening. This stands in contrast to assessment of drug absorption for which *in vitro* screens with intestinal epithelial cells lines (eg, Caco-2) are ubiquitous and indispensable for drug discovery. One possible explanation is that monocultures may be too simple to replicate the integrated function of diverse epithelial cell types and are therefore unable to capture diverse GI toxicities. Here, we describe a human GI microtissue comprised of diverse epithelial cell types grown on a fibroblast substrate that can detect with good predictivity compounds that induce diarrhea in humans.

The initial priority for microtissue evaluation was to investigate aspects of clinical translation. For the validation set, the central goal was testing translational accuracy. Therefore, widely prescribed drugs were selected to ensure that robust clinical data underpinned the accuracy assessment. Importantly, the data revealed a predictive accuracy of 80% which matches the translation accuracy of *in vivo* studies in higher-order species (Monticello *et al.*, 2017; Olson *et al.*, 2000).

As a follow up, translational limitations were investigated based on the reasoning that drugs that failed or were significantly impacted in the clinic by dose-limiting diarrhea may be instances where the existing preclinical models underestimated the GI risk. As it happens, the scope of such a test is limited by access to data on failed compounds in the public domain. In the AstraZeneca collection, four such compounds were identified. Each had been tested in 1-month toxicity studies in both rat and dog. These animal studies generally underpredicted the clinical diarrhea observed for these compounds. In dogs, GIT was noted as the maximum tolerated dose (MTD) for one compound (AZD3409) whereas in rats, GIT was the DLT for a different compound (AZD8931). In contrast, all four compounds were positive in TEER as classified by TEER/C_{max} ratios ≤ 8, well below the threshold of < 80 observed with approved drugs (Table 5). Whereas this sample size is limited, the data suggest the translation accuracy and sensitivity requisite for preclinical testing is not limited to marketed drugs. The implied translational advantage for human microtissues relative to animal studies will require further testing.

The relationship between *in vitro* assay potency and clinical exposure is important for defining the safety margin (Keating *et al.*, 2014). The present model exhibited an 80-fold margin between the minimum TEER response and the maximum clinical concentration associated with diarrhea. This is in a similar range with an *ex vivo* mouse colon organ bath assay which found a 50-fold margin as optimal (Keating *et al.*, 2014). This margin is also in line with other nonGI settings, notably cardiovascular, where a 30 to 100-fold ratio of hERG potency to C_{max} is optimal depending on the disease indication (Redfern *et al.*, 2003).

In addition to the need for predictive assays to screen out off-target GIT, a second key demand is for assays that can inform clinical strategies to manage on-target GIT. Emerging modeling approaches can exploit differences in the dynamics of toxicity and efficacy responses by optimizing compound pharmacokinetics or refining clinical dosing schedules (Venkatakrishnan *et al.*, 2015). A second related demand for *in vitro* kinetic data stems from cancer therapeutics for which on-target GITs are pervasive as monotherapy and are exacerbated by the standard practice of combination therapy. Modeling response dynamics may guide selection of combination drug pairings or schedules to improve tolerability.

Developing dynamic mathematical models requires data that resolves response kinetics. TEER data is label-free and thus consistent with repeated measurement. The ability to generate kinetic response profiles with microtissue TEER was explored with washout studies using two diarrheagenic compounds (AZD1 and AZD8931) and one nondiarrheagenic (AZD2). Differences in the onset and particularly recovery of TEER effects were readily distinguished between doses and schedules. This feasibility test demonstrated that microtissue

Table 4. Using the TEER IC$_{15}$/C$_{max}$ Ratio < 80 As Diarrhea-Genic Criteria, Measures of Diagnostic Accuracy Were Calculated for Three-Independent Experiments Testing the Validation Set in the Human GI Microtissue (Exp 1, Exp 2) or Caco-2 TEER Assay (Table 3)

	TEER Exp 1	TEER Exp 2	MTT Exp 2	TEER Caco-2
Cmpds	31	30	31	31
Sensitivity	79%	71%	**50%**	**57%**
Specificity	88%	94%	100%	94%
Accuracy	84%	83%	77%	77%

Table 5. Nonmarketed Drugs With High Incidence of Clinical Diarrhea That Was Not Consistently Predicted by Preclinical 1-Month Animal Studies

CD	Clinical Diarrhea Incidence	Rat 1 Month Findings	Dog 1 Month Findings	TEER (IC$_{15}$)	Clinical C$_{max}$	TEER Diarrhea-Genic Prediction (IC$_{15}$/C$_{max}$)
AZD3409	41% (12/29)	GIT not noted at MTD	GIT at MTD	3.0E-06	3.9E-07	Active (8)
AZD8931	51% (61/120)	DLT: GIT	GIT not noted at MTD	3.0E-9	1.3E-07	Active (0.02)
AZD7140	60% (9/15)	GIT not noted at MTD	Occasion soft feces at highest dose	3.0E-06	3.6E-06	Active (0.8)
AZD3	33% (8/24)	GIT not noted at MTD	GIT not noted at MTD	2.0E-08	8.4E-07	Active (0.02)

Predictive clinical outcomes with human GI microtissue TEER were scored using TEER IC$_{15}$/C$_{max}$ ratio < 80 as diarrhea-genic criteria. C$_{max}$ values associated with diarrhea were used. Experiments were conducted under blinded conditions.
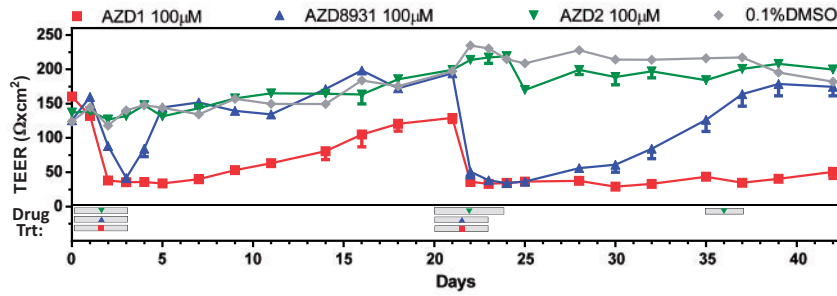
Figure 4. Assessment of GI microtissue TEER responses kinetics. Response on-set and recovery was evaluated after initial treatment, washout, and repeat treatments. The interval of continuous drug treatment prior to washout is denoted by a shaded bar with the corresponding symbol. Experiments were conducted under blinded conditions. All data points include error bars are plotted at standard error of mean of triplicates.
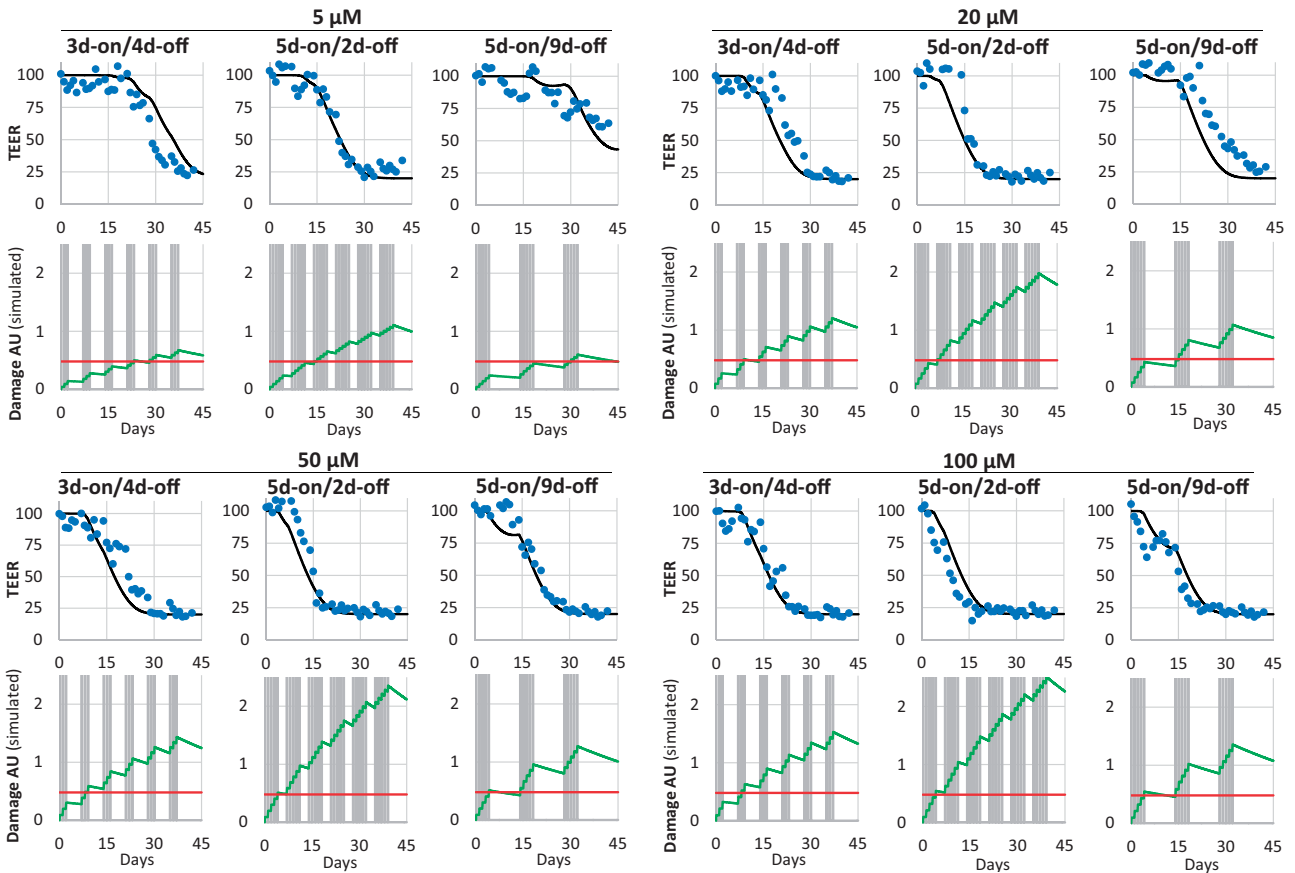

Figure 5. Dose schedule exploration. TEER measurements (upper plots) and model predictions for TEER (upper plots) and barrier damage (stepped lines, AU: arbitrary units) for human GI microtissues exposed to AZD1 for 150 min daily according to clinically proposed dosing schedules (gray bars). A threshold in damage (horizontal line) was associated with TEER disruption.

TEER delivers each of five critical data features essential for kinetic investigation including: (1) inter-day consistency, (2) compatibility with drug washout, (3) viability for extended duration (42 days), (4) compatibility with repeat dosing, all of which while (5) retaining sensitivity to differences in response on-set and recovery.

To challenge TEER data for the capacity to support mathematical modeling, AZD1 was retested using clinically relevant exposure levels, durations, and schedules. TEER data from 12 dose levels-schedules pairings was explained by a simple mathematical model and revealed unappreciated response dynamics. A distinctive delay from exposure to the initial decrease in TEER was

discovered. Whereas the absolute delay varied with different treatments, mathematical modeling revealed a remarkably consistent exposure-response relationship. TEER decreased only when accumulated epithelial damage reached a threshold value. Recovery from AZD1-induced damage was slow relative to the rate damage accumulation suggesting that long exposure holidays would be required for recovery (Figure 5). Clinical data is not available to evaluate the *in vitro* to clinical translation and further work is required to demonstrate the translational nature of these mathematical models into the *in vivo* setting. Nevertheless, our results demonstrate the ability of microtissue TEER combined with mathematical modeling to predict complex epithelial

responses comprising damage, recovery, and sensitization over time at clinically relevant dose schedules.

The potential impact of being able to guide clinical plans to increase therapeutic index is significant and merits detailed consideration of improvements that could refine kinetic data collection and modeling accuracy. The current microtissue TEER assay introduces two strengths relative to enteroids. The transwell format enables drug access to basal or apical sides and allows easy washout. The TEER endpoint enables repeat re-reading in contrast to destructive cytotoxicity endpoint assays. There may be opportunities to extend these advances. Currently, TEER instruments use silver electrodes, hence it is recommended that the cell culture media be replaced with KCl buffer during the reading period. Measurement of barrier function utilizing gold electrodes, such as with impedance, enables reading in cell culture media. There is broad precedent for impedance platforms delivering exquisite sensitivity and robust data suitable in other areas of drug discovery—eg, cardiotoxicity and complex GPCR pharmacology (Guo et al., 2013; Scott and Peters, 2010). For GI applications, impedance with gold electrodes delivered robust real-time tracking of barrier function with a mouse colonic epithelial cell line cultured on a solid surface (Haines et al., 2016). A future platform uniting continuous real-time monitoring and transwell ALI cultures with human GI microtissue would be a valuable advance.

Because a validated in vitro GIT assay is unprecedented, the field will need an accumulation of experience to understand limitations and refine the application. This study investigated suitability of the human GI microtissue TEER assay for detecting disruption of barrier function and predicting diarrhea. Whereas there is no expectation of predictivity for other GI toxicities, it should be noted that while assembling a nausea-genic validation set, Parkinson et al. (2012) found that vomiting, diarrhea, and hyper-salivation co-occurred with sufficient frequency for predictive utility. Likewise, one would expect an epithelial-only model to miss GITs mediated by mechanisms involving enteric nerves or smooth muscle (eg, altered intestinal mobility) or immune cells (eg, colitis). However, toxicity mechanisms that exclude epithelial effects may be less common when considering off-target drug-induced GIT, which is consistent with the low number of false negatives in the present assay.

Diverse opportunities for refining in vitro GIT assays are rapidly emerging. Examining the strengths of novel platforms will be a priority. For example, intestinal stem cells have been cloned that display exquisitely precise, cell-autonomous commitment to epithelial differentiation consistent with the region of origin (Wang et al., 2015). This advance offers potential for assays with intestinal region-specific microtissues and to investigate the molecular basis for regional-selective GI toxicity. Customized assays for orally versus intravenously administered drugs may be possible with refined apical-to-basal drug concentration gradients. Although the present assay platform delivered accuracy greater than 80%, drugs with variable incidence ($< 40\%$) were not considered and may offer valuable tools to demonstrate the added value of region-specific or apical-to-basal drug concentration gradients.

With respect to mechanistic limitations of microtissue assays, developing this understanding will require tandem advances that elucidate the underlying toxicity signaling pathways and identify more selective tool compounds to test these pathways. Seven targets/pathways expressed in enterocytes and linked to GI dysfunction are candidates that merit investigation (reviewed in [Camilleri et al., 2016]) however selective tool compounds with defined clinical translation are lacking.

Similarly, selective agents are needed to test effects of pharmacological regulation of tight-junctions in GI microtissue (Odenwald and Turner, 2017). As screening limitations are defined, targeted improvements in GI microtissues may be possible utilizing the rapidly emerging understanding of chemical gradients driving crypt-villus axis (Wang et al., 2018).

To our knowledge this human 3D GI microtissue is the first in vitro assay validated for GI drug safety testing; with moderate throughput the 96-well assay should provide a platform for lead optimization and dose schedule exploration. Thus, there is rationale for optimism that a new era of in vitro GIT testing may be imminent. The present findings demonstrate that in vitro assays can incorporate six features important for routine screening including: (1) diverse epithelial cell types organized as microtissues emanating from stem cells, (2) cells derived from a higher-order species, particularly human, (3) a functional endpoint linked to core tissue function (eg, epithelia barrier function for diarrhea), (4) clinical translation, (5) sufficient throughput (eg, 96-well), and (6) capacity for quantifying dynamics of toxicity onset and recovery. Assays with these attributes should enable GI drug safety screening to reduce GIT frequency and manage the impact of this liability in the clinic.

SUPPLEMENTARY DATA

Supplementary data are available at Toxicological Sciences online.

ACKNOWLEDGMENTS

FUNDING

REFERENCES

Abraham, B., and Sellin, J. H. (2007). Drug-induced diarrhea. Curr. Gastroenterol. Rep. 9, 365–372.

Abraham, B. P., and Sellin, J. H. (2012). Drug-induced, factitious, & idiopathic diarrhoea. Best Pract. Res. Clin. Gastroenterol. 26, 633–648.

Al-Saffar, A., Nogueira da Costa, A., Delaunois, A., Leishman, D. J., Marks, L., Rosseels, M. L., and Valentin, J. P. (2015). Gastrointestinal safety pharmacology in drug discovery and development. Handb. Exp. Pharmacol. 229, 291–321.

Appels, N. M., Bolijn, M. J., Chan, K., Stephens, T. C., Hoctin-Boes, G., Middleton, M., Beijnen, J. H., de Bono, J. S., Harris, A. L., and Schellens, J. H. (2008). Phase I pharmacokinetic and pharmacodynamic study of the prenyl transferase inhibitor AZD3409 in patients with advanced cancer. Br. J. Cancer 98, 1951–1958.

Ayehunie, S., Landry, T., Stevens, Z., Armento, A., Hayden, P., and Klausner, M. (2018). Human primary cell-based organotypic microtissues for modeling small intestinal drug absorption. Pharm. Res. 35, 72.

Blutt, S. E., Broughman, J. R., Zou, W., Zeng, X. L., Karandikar, U. C., In, J., Zachos, N. C., Kovbasnjuk, O., Donowitz, M., and

Estes, M. K. (2017). Gastrointestinal microphysiological systems. *Exp. Biol. Med. (Maywood)* **242**, 1633–1642.

Boccellato, F., Woelffling, S., Imai-Matsushima, A., Sanchez, G., Goosmann, C., Schmid, M., Berger, H., Morey, P., Denecke, C., Ordemann, J., et al. (2018). Polarised epithelial monolayers of the gastric mucosa reveal insights into mucosal homeostasis and defence against infection. *Gut* doi: 10.1136/gutjnl-2017-314540.

Cadoo, K. A., Gajria, D., Suh, E., Patil, S., Theodoulou, M., Norton, L., Hudis, C. A., and Traina, T. A. (2016). Decreased gastrointestinal toxicity associated with a novel capecitabine schedule (7 days on and 7 days off): A systematic review. *NPJ Breast Cancer* **2**, 16006.

Camilleri, M., Bueno, L., Andresen, V., De Ponti, F., Choi, M. G., and Lembo, A. (2016). Pharmacological, pharmacokinetic, and pharmacogenomic aspects of functional gastrointestinal disorders. *Gastroenterology* doi: 10.1053/j.gastro.2016.02.029.

Cook, D., Brown, D., Alexander, R., March, R., Morgan, P., Satterthwaite, G., and Pangalos, M. N. (2014). Lessons learned from the fate of AstraZeneca's drug pipeline: A five-dimensional framework. *Nat. Rev. Drug Discov.* **13**, 419–431.

Dekkers, J. F., Wiegerinck, C. L., de Jonge, H. R., Bronsveld, I., Janssens, H. M., de Winter-de Groot, K. M., Brandsma, A. M., de Jong, N. W., Bijvelds, M. J., Scholte, B. J., et al. (2013). A functional CFTR assay using primary cystic fibrosis intestinal organoids. *Nat. Med.* **19**, 939–945.

Fatehullah, A., Tan, S. H., and Barker, N. (2016). Organoids as an *in vitro* model of human development and disease. *Nat. Cell Biol.* **18**, 246–254.

Federer, C., Yoo, M., and Tan, A. C. (2016). Big data mining and adverse event pattern analysis in clinical drug trials. *Assay Drug Dev. Technol.* **14**, 557–566.

Fujii, S., Suzuki, K., Kawamoto, A., Ishibashi, F., Nakata, T., Murano, T., Ito, G., Shimizu, H., Mizutani, T., Oshima, S., et al. (2016). PGE2 is a direct and robust mediator of anion/fluid secretion by human intestinal epithelial cells. *Sci. Rep.* **6**, 36795.

Gamucci, T., Moscetti, L., Mentuccia, L., Pizzuti, L., Mauri, M., Zampa, G., Pavese, I., Sperduti, I., Vaccaro, A., and Vici, P. (2014). Optimal tolerability and high efficacy of a modified schedule of lapatinib-capecitabine in advanced breast cancer patients. *J. Cancer Res. Clin. Oncol.* **140**, 221–226.

Gebremichael, Y., Lu, J., Shankaran, H., Helmlinger, G., Mettetal, J., and Hallow, K. M. (2018). Multiscale mathematical model of drug-induced proximal tubule injury: Linking urinary biomarkers to epithelial cell injury and renal dysfunction. *Toxicol. Sci.* **162**, 200–211.

Genschow, E., Spielmann, H., Scholz, G., Seiler, A., Brown, N., Piersma, A., Brady, M., Clemann, N., Huuskonen, H., Paillard, F., et al. (2002). The ECVAM international validation study on *in vitro* embryotoxicity tests: Results of the definitive phase and evaluation of prediction models. European Centre for the Validation of Alternative Methods. *Altern. Lab. Anim.* **30**, 151–176.

Grabinger, T., Luks, L., Kostadinova, F., Zimberlin, C., Medema, J. P., Leist, M., and Brunner, T. (2014). Ex vivo culture of intestinal crypt organoids as a model system for assessing cell death induction in intestinal epithelial cells and enteropathy. *Cell Death Dis.* **5**, e1228.

Guengerich, F. P. (2011). Mechanisms of drug toxicity and relevance to pharmaceutical development. *Drug Metab. Pharmacokinet.* **26**, 3–14.

Guo, L., Coyle, L., Abrams, R. M., Kemper, R., Chiao, E. T., and Kolaja, K. L. (2013). Refining the human iPSC-cardiomyocyte arrhythmic risk assessment model. *Toxicol. Sci.* **136**, 581–594.

Haines, R. J., Beard, R. S., Jr, Eitner, R. A., Chen, L., and Wu, M. H. (2016). TNFalpha/IFNgamma mediated intestinal epithelial barrier dysfunction is attenuated by microRNA-93 downregulation of PTK6 in mouse colonic epithelial cells. *PLoS One* **11**, e0154351.

Hoyle, S., Bonavita, A. M., Murdoch, A., Brown, M., Howard, W., and Booth, C. (2016). Validation of human, rat and mouse intestinal organoid models as preclinical screens to assess GI toxicity in novel oncology drug development. *Eur. Organ. Res. Treat. Cancer* **69**, S77.

Ito, S., and Karnovsky, M. J. (1968). Formaldehyde-glutaraldehyde fixative containing trinitro compounds. *J. Cell Biol.* **39**, 168.

Johnston, S., Basik, M., Hegg, R., Lausoontornsiri, W., Grzeda, L., Clemons, M., Dreosti, L., Mann, H., Stuart, M., and Cristofanilli, M. (2016). Inhibition of EGFR, HER2, and HER3 signaling with AZD8931 in combination with anastrozole as an anticancer approach: Phase II randomized study in women with endocrine-therapy-naive advanced breast cancer. *Breast Cancer Res. Treat.* **160**, 91–99.

Keating, C., Ewart, L., Grundy, L., Valentin, J. P., and Grundy, D. (2014). Translational potential of a mouse *in vitro* bioassay in predicting gastrointestinal adverse drug reactions in Phase I clinical trials. *Neurogastroenterol. Motil.* **26**, 980–989.

Konsoula, R., and Barile, F. A. (2007). Correlation of *in vitro* cytotoxicity with paracellular permeability in mortal rat intestinal cells. *J. Pharmacol. Toxicol. Methods* **55**, 176–183.

Li, X., Nadauld, L., Ootani, A., Corney, D. C., Pai, R. K., Gevaert, O., Cantrell, M. A., Rack, P. G., Neal, J. T., Chan, C. W.-M., et al. (2014). Oncogenic transformation of diverse gastrointestinal tissues in primary organoid culture. *Nat. Med.* **20**, 769–777.

Li, X., Ootani, A., and Kuo, C. (2016). An air-liquid interface culture system for 3D organoid culture of diverse primary gastrointestinal tissues. *Methods Mol. Biol.* **1422**, 33–40.

Lin, Z., and Will, Y. (2012). Evaluation of drugs with specific organ toxicities in organ-specific cell lines. *Toxicol. Sci.* **126**, 114–127.

Llavero-Valero, M., Guillen-Grima, F., Zafon, C., and Galofre, J. C. (2016). The placebo effect in thyroid cancer: A meta-analysis. *Eur. J. Endocrinol.* **174**, 465–472.

Maschmeyer, I., Hasenberg, T., Jaenicke, A., Lindner, M., Lorenz, A. K., Zech, J., Garbe, L. A., Sonntag, F., Hayden, P., Ayehunie, S., et al. (2015). Chip-based human liver-intestine and liver-skin co-cultures—A first step toward systemic repeated dose substance testing *in vitro*. *Eur. J. Pharm. Biopharm.* **95**, 77–87.

Monticello, T. M., Jones, T. W., Dambach, D. M., Potter, D. M., Bolt, M. W., Liu, M., Keller, D. A., Hart, T. K., and Kadambi, V. J. (2017). Current nonclinical testing paradigm enables safe entry to First-in-Human clinical trials: The IQ consortium nonclinical to clinical translational database. *Toxicol. Appl. Pharmacol.* **334**, 100–109.

Nossol, C., Diesing, A. K., Walk, N., Faber-Zuschratter, H., Hartig, R., Post, A., Kluess, J., Rothkotter, H. J., and Kahlert, S. (2011). Air-liquid interface cultures enhance the oxygen supply and trigger the structural and functional differentiation of intestinal porcine epithelial cells (IPEC). *Histochem. Cell Biol.* **136**, 103–115.

Odenwald, M. A., and Turner, J. R. (2017). The intestinal epithelial barrier: A therapeutic target? *Nat. Rev. Gastroenterol. Hepatol.* **14**, 9–21.

Olson, H., Betton, G., Robinson, D., Thomas, K., Monro, A., Kolaja, G., Lilly, P., Sanders, J., Sipes, G., Bracken, W., et al. (2000). Concordance of the toxicity of pharmaceuticals in humans and in animals. *Regul. Toxicol. Pharmacol.* **32**, 56–67.

Ootani, A., Li, X., Sangiorgi, E., Ho, Q. T., Ueno, H., Toda, S., Sugihara, H., Fujimoto, K., Weissman, I. L., Capecchi, M. R., *et al.* (2009). Sustained *in vitro* intestinal epithelial culture within a Wnt-dependent stem cell niche. *Nat. Med.* **15**, 701–706.

Parkinson, J., Muthas, D., Clark, M., Boyer, S., Valentin, J. P., and Ewart, L. (2012). Application of data mining and visualization techniques for the prediction of drug-induced nausea in man. *Toxicol. Sci.* **126**, 275–284.

Redfern, W. S., Carlsson, L., Davis, A. S., Lynch, W. G., MacKenzie, I., Palethorpe, S., Siegl, P. K., Strang, I., Sullivan, A. T., and Wallis, R. (2003). Relationships between preclinical cardiac electrophysiology, clinical QT interval prolongation and torsade de pointes for a broad range of drugs: Evidence for a provisional safety margin in drug development. *Cardiovasc. Res.* **58**, 32–45.

Rief, W., Avorn, J., and Barsky, A. J. (2006). Medication-attributed adverse effects in placebo groups: Implications for assessment of adverse effects. *Arch. Intern. Med.* **166**, 155–160.

Sato, T., Vries, R. G., Snippert, H. J., van de Wetering, M., Barker, N., Stange, D. E., van Es, J. H., Abo, A., Kujala, P., Peters, P. J., *et al.* (2009). Single Lgr5 stem cells build crypt-villus structures *in vitro* without a mesenchymal niche. *Nature* **459**, 262–265.

Scott, C. W., and Peters, M. F. (2010). Label-free whole-cell assays: Expanding the scope of GPCR screening. *Drug Discov. Today* **15**, 704–716.

Shankaran, H., Cronin, A., Barnes, J., Sharma, P., Tolsma, J., Jasper, P., and Mettetal, J. T. (2018). Systems pharmacology model of gastrointestinal damage predicts species differences and optimizes clinical dosing schedules. *CPT Pharmacometrics Syst. Pharmacol.* **7**, 26–33.

Srinivasan, B., Kolli, A. R., Esch, M. B., Abaci, H. E., Shuler, M. L., and Hickman, J. J. (2015). TEER measurement techniques for *in vitro* barrier model systems. *J. Lab. Autom.* **20**, 107–126.

Stein, A., Voigt, W., and Jordan, K. (2010). Chemotherapy-induced diarrhea: Pathophysiology, frequency and guideline-based management. *Ther. Adv. Med. Oncol.* **2**, 51–63.

Stevens, J. L., and Baker, T. K. (2009). The future of drug safety testing: Expanding the view and narrowing the focus. *Drug Discov. Today* **14**, 162–167.

Venkatakrishnan, K., Friberg, L. E., Ouellet, D., Mettetal, J. T., Stein, A., Troconiz, I. F., Bruno, R., Mehrotra, N., Gobburu, J., and Mould, D. R. (2015). Optimizing oncology therapeutics through quantitative translational and clinical pharmacology: Challenges and opportunities. *Clin. Pharmacol. Ther.* **97**, 37–54.

Wang, Y., Gunasekara, D. B., Reed, M. I., DiSalvo, M., Bultman, S. J., Sims, C. E., Magness, S. T., and Allbritton, N. L. (2017). A microengineered collagen scaffold for generating a polarized crypt-villus architecture of human small intestinal epithelium. *Biomaterials* **128**, 44–55.

Wang, Y., Kim, R., Hinman, S. S., Zwarycz, B., Magness, S. T., and Allbritton, N. L. (2018). Bioengineered systems and designer matrices that recapitulate the intestinal stem cell niche. *Cell. Mol. Gastroenterol. Hepatol.* **5**, 440–453 e1.

Wang, X., Yamamoto, Y., Wilson, L. H., Zhang, T., Howitt, B. E., Farrow, M. A., Kern, F., Ning, G., Hong, Y., Khor, C. C., *et al.* (2015). Cloning and variation of ground state intestinal stem cells. *Nature* **522**, 173–178.

Yin, X., Mead, B. E., Safaee, H., Langer, R., Karp, J. M., and Levy, O. (2016). Engineering stem cell organoids. *Cell Stem Cell* **18**, 25–38.

Youden, W. J. (1950). Index for rating diagnostic tests. *Cancer* **3**, 32–35.